

# Inelastic neutron scattering studies of Crystal Field Levels in $\text{PrOs}_4\text{As}_{12}$

Songxue Chi,<sup>1</sup> Pengcheng Dai,<sup>1,2</sup> T. Barnes,<sup>1,2</sup> H. J. Kang,<sup>3</sup> J. W. Lynn,<sup>3</sup>

R. Bewley,<sup>4</sup> F. Ye,<sup>2</sup> M. B. Maple,<sup>5</sup> Z. Henkie,<sup>6</sup> and A. Pietraszko<sup>6</sup>

<sup>1</sup>*Department of Physics and Astronomy, The University of Tennessee, Knoxville, Tennessee 37996-1200, USA*

<sup>2</sup>*Oak Ridge National Laboratory, Oak Ridge, Tennessee 37831, USA*

<sup>3</sup>*NIST Center for Neutron Research, National Institute of Standards and Technology, Gaithersburg, Maryland 20899-6102, USA*

<sup>4</sup>*Rutherford Appleton Laboratory, Chilton, Didcot, Oxon. OX11 0QX, UK*

<sup>5</sup>*Department of Physics, University of California at San Diego, La Jolla, California 92093, USA*

<sup>6</sup>*Institute of Low Temperature and Structure Research,  
Polish Academy of Science, 50-950 Wrocław, Poland*

(Dated: February 20, 2008)

We use neutron scattering to study the  $\text{Pr}^{3+}$  crystalline electric field (CEF) excitations in the filled skutterudite  $\text{PrOs}_4\text{As}_{12}$ . By comparing the observed levels and their strengths under neutron excitation with the theoretical spectrum and neutron excitation intensities, we identify the  $\text{Pr}^{3+}$  CEF levels, and show that the ground state is a magnetic  $\Gamma_4^{(2)}$  triplet, and the excited states  $\Gamma_1$ ,  $\Gamma_4^{(1)}$  and  $\Gamma_{23}$  are at 0.4, 13 and 23 meV, respectively. A comparison of the observed CEF levels in  $\text{PrOs}_4\text{As}_{12}$  with the heavy fermion superconductor  $\text{PrOs}_4\text{Sb}_{12}$  reveals the microscopic origin of the differences in the ground states of these two filled skutterudites.

PACS numbers: 75.47.-m, 71.70.Ch

## I. INTRODUCTION

The Pr-based filled skutterudites (FS) have the formula  $\text{PrT}_4\text{X}_{12}$ , where T is one of the transition metals Fe, Ru, or Os, and X is a pnictogen (P, As, or Sb)<sup>1,2,3</sup>. The notably mounting interests and efforts in the study of the FS compounds are motivated by the remarkable diversity of their electronic and magnetic ground states, including multipole ordering<sup>4,5</sup>, small gap insulators<sup>6,7</sup>, conventional superconductivity<sup>8,9</sup>, unconventional superconductivity<sup>10,11</sup> and magnetic ordering<sup>12,13,14,15,16</sup>. Despite the large differences in their physical properties, these compounds are governed by only a few parameters, including the interaction between the conduction and the 4f shell electrons (the c-f coupling) and the effect of the crystalline electric field (CEF) potential on the  $\text{Pr}^{3+}$  4f electrons<sup>4,5,6,7,10,11,12,13,14,15,16</sup>. For example, transport and bulk magnetic measurements on the heavy Fermion superconductor  $\text{PrOs}_4\text{Sb}_{12}$  suggested either a  $\Gamma_1$  singlet ground state or a  $\Gamma_3$  nonmagnetic doublet ground state<sup>10,11</sup>. Inelastic neutron scattering experiments on  $\text{PrOs}_4\text{Sb}_{12}$  showed that the  $\text{Pr}^{3+}$  CEF levels include a  $\Gamma_1$  singlet ground state and a low-lying  $\Gamma_4^{(2)}$  magnetic triplet excited state at 0.6 meV<sup>18,19,20</sup>. This rules out the quadrupolar Kondo effect, which arises only from a nonmagnetic doublet ground state<sup>17</sup>, as the microscopic origin for the observed heavy-fermion superconductivity.

The FS compounds belong to the space group  $\text{Im}\bar{3}$ . The rare earth atoms are located at the corners and body-center of the cubic lattice, each of which is surrounded by a simple cube of 8 transition metal atoms at the 8c sites [Fig. 1(a)] and by an icosahedron of 12 pnictogen atoms at the 24g Wyckoff sites [Fig. 1(c)]. Owing to their unique structure, a subtle modification on composition can result in a different CEF scheme and thus

a completely different ground state. However, a general understanding is desirable as to how the compositions influence the CEF levels. In  $\text{PrOs}_4\text{As}_{12}$ , in which the pnictogen Sb in  $\text{PrOs}_4\text{Sb}_{12}$  is replaced by As, the material displays quite different correlated electron properties<sup>14,15</sup>. The temperature dependence of the electrical resistivity reveals Kondo lattice behavior, which is not observed in  $\text{PrOs}_4\text{Sb}_{12}$ <sup>21</sup>. Specific heat measurements indicate an enhanced electronic specific heat coefficient of  $\gamma \approx 1 \text{ J/mol K}^2$  for  $T \leq 1.6 \text{ K}$  and  $0 \leq H \leq 1.25 \text{ T}^{14}$ . The compound exhibits several ordered phases at temperatures below 2.3 K and fields below about 3 T<sup>22</sup>. The ground state has been determined to be antiferromagnetic (AF) by neutron scattering experiments<sup>15</sup>. A determination of the  $\text{Pr}^{3+}$  CEF level scheme in  $\text{PrOs}_4\text{As}_{12}$  and its microscopic origin is crucial for understanding why its ground state is different from that in  $\text{PrOs}_4\text{Sb}_{12}$ . The outcome will lead to a more general understanding of how the structures and compositions in Pr-based FSs can influence their CEF levels and ground states.

## II. EXPERIMENTAL

$\text{PrOs}_4\text{As}_{12}$  single crystals were grown using the molten metal flux method described in Ref.<sup>14</sup> and crushed into fine powder. Our neutron scattering experiments were carried out on the cold neutron triple-axis spectrometer SPINS at the NIST Center for Neutron Research (NCNR) and on the HET chopper spectrometer at ISIS (Rutherford Appleton Laboratory), as described previously<sup>23</sup>. We reference positions in reciprocal space at wave vector  $\mathbf{Q} = (q_x, q_y, q_z)$  in  $\text{\AA}^{-1}$  using  $(H, K, L)$  reciprocal lattice units (r.l.u.) notation, where  $(H, K, L) = (q_x a/2\pi, q_y a/2\pi, q_z a/2\pi)$  for the cubic  $\text{PrOs}_4\text{As}_{12}$  unit cell ( $a = 8.5319 \text{ \AA}$ )<sup>14</sup>. We used a  $^3\text{He}$ - $^4\text{He}$  dilution refrigerator for the field-dependent experiments. The nature of observed CEF excitations were

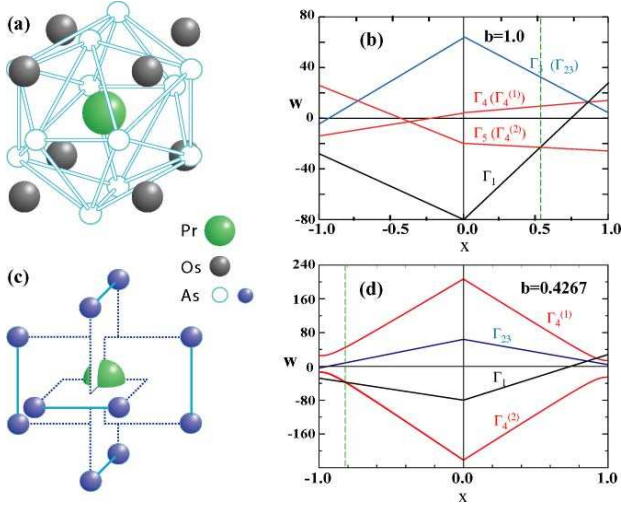


FIG. 1: (Color online) (a) The cube of 8 Os ions surrounding the central  $\text{Pr}^{3+}$  ion in  $\text{PrOs}_4\text{As}_{12}$ . These give an  $O_h$ -symmetric CEF. (b) The corresponding spectrum of  $O_h$ -symmetry  $\text{Pr}^{3+}$  CEF levels. (black=singlet, blue=doublet, red=triplet). The relative coupling  $x$  that gives singlet-triplet degeneracy is shown by a dashed vertical. (c) The 12 nearest-neighbor As ions surrounding the central  $\text{Pr}^{3+}$  in  $\text{PrOs}_4\text{As}_{12}$ , giving a reduced symmetry ( $T_h$ ) CEF. (d) The corresponding As-only  $T_h$ -symmetry  $\text{Pr}^{3+}$  CEF spectrum in  $\text{PrOs}_4\text{As}_{12}$ .

confirmed in a large temperature (0.08 K-200 K) and magnetic field (0 T-11 T) range.

### III. RESULTS AND DISCUSSION

Figure 2 summarizes the neutron scattering intensity from  $\text{PrOs}_4\text{As}_{12}$  on HET at temperatures between 1.5 K and 200 K. Since the CEF magnetic scattering decreases with increasing  $Q$  whereas the intensity of phonons increases with  $Q$ , a comparison of the neutron intensities in the low- and high-angle detectors can distinguish between magnetic and phonon scattering. Figure 2a shows the scattering function at  $T = 1.5$  K and  $T = 200$  K with an incident neutron beam energy of  $E_i = 32$  meV. Comparison of the low- and high-angle data reveals two clear CEF excitations at 13 meV and 23 meV, with phonons at  $\sim 20$  meV. Measurements with  $E_i = 12$  and 50 meV showed no evidence of additional CEF excitations at energy transfers between 2 and 8 meV or above 25 meV [Figs. 2(b) and 2(c)].

To search for CEF excitations at energies below 2 meV, we carried out high resolution measurements using SPINS. At  $T = 0.32$  K, energy scans at  $Q = (1.2, 0, 0)$  showed a clear peak at 0.4 meV; this mode decreases and becomes broader on warming to 2.5 K and 6 K [Fig. 3(a)]. Figure 3(b) shows that the energy of the  $\sim 0.4$  meV mode has weak  $Q$ -dependence and decreases in intensity with increasing  $Q$ , thus confirming its magnetic nature. Figure 3(d) reveals that the elastic intensity also decreases on warming from 0.08 K to 4 K. This reduction of intensity in the elastic channel with increasing temperature is

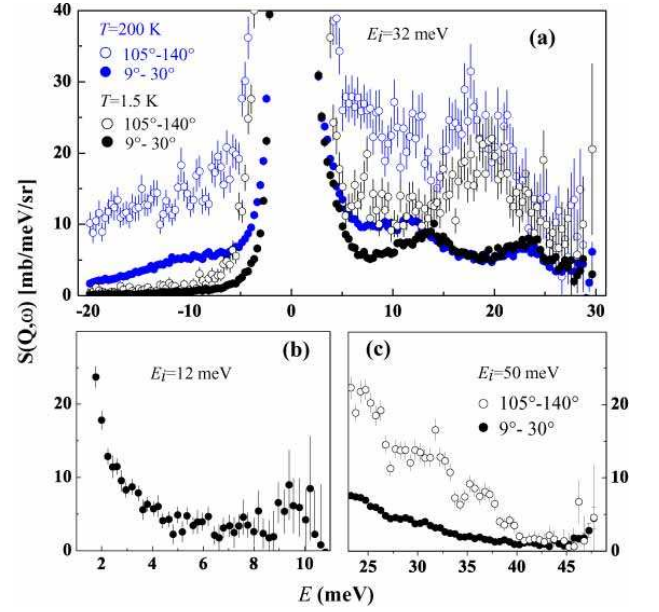


FIG. 2: (Color online) (a) Neutron inelastic scattering at  $T = 1.5$  K and  $T = 200$  K with  $E_i = 32$  meV, integrated over scattering angles from  $9^\circ$  to  $30^\circ$  (low-angle detectors) and from  $105^\circ$  to  $140^\circ$  (high-angle detectors). (b) The same at  $E_i = 12$  meV; (c)  $E_i = 50$  meV. The scattering function  $S(Q, \omega)$  was normalized by comparison to a vanadium standard.

also observed in the HET data, evidencing the ground state is a magnetic multiplet.

Figures 4(a)-(d) show the temperature dependence of the low-angle scattering for  $E_i = 32$  meV. The CEF peak intensities do not change significantly with temperature between 1.5 K and 5 K. At 50 K the intensity in the elastic channel has undergone a substantial decrease, and the 13 meV peak has shifted to 10 meV. On further increasing the temperature to 100 K and 200 K the intensities at 0 meV, 13 meV and 23 meV continue to decrease, whereas the scattering at 10 meV increases.

The theoretical description of the  $\text{Pr}^{3+}$  CEF levels in  $\text{PrOs}_4\text{As}_{12}$  is complicated by the presence of important contributions from two sets of neighboring ions, Os and As. The  $\text{Pr}^{3+}$  ion in Pr-based FS has a  $4f^2$  configuration, which in Russell-Saunders coupling has a ninefold degenerate  $^3\text{H}_4$  ground state. This degeneracy is lifted by the CEF interaction, which we assume to be dominated by the 12 nearest neighbor pnictogens (As) and the 8 next nearest neighbor Os ions; the distances to these ions are  $d_{\text{Pr-As}} = 3.23$  Å and  $d_{\text{Pr-Os}} = 3.69$  Å respectively.

#### A. Single – charge model with separate ions

Os ions form a simple cube around the Pr ions and they alone give an  $O_h$  symmetric CEF. The arrangement of the 12 pnictogens (As) around  $\text{Pr}^{3+}$  forms 3 orthogonally intersected planes where the As-As bonds are shown as solid lines with length  $L$  and  $W$  is the length of the dashed lines in Fig. 1(c) ( $b = W/L = 0.4267 \neq 1$ ). When

the 4 pnictogen atoms in each of the 3 orthogonally intersected planes form a square, *i.e.*,  $b = W/L = 1$ , the fourfold rotational symmetry is recovered and the point group symmetry becomes  $O_h$  with the simple cubic CEF potentials [Fig. 1(c)]<sup>26</sup>. This  $O_h$  case is treated by Lea, Leask, and Wolf (LLW)<sup>26</sup> (see their Fig. 9); we have re-derived their excitation spectrum as shown in Fig. 1(b).

Both  $O_h$  and  $T_h$  CEF interactions split the  $\text{Pr}^{3+} {}^3\text{H}_4$  ground state into a singlet, a doublet and two triplets<sup>25</sup>. In the  $b \neq 1$   $T_h$ -symmetry case, these multiplets are referred to as  $\Gamma_1$  (a singlet),  $\Gamma_{23}$  (a nonmagnetic doublet), and  $\Gamma_4^{(1)}$  and  $\Gamma_4^{(2)}$  (magnetic triplets). These two triplets are linear combinations of the  $O_h$ -symmetry triplets, mixed by the new  $T_h$  CEF interaction<sup>25</sup>; this mixing modifies the excitation spectrum and leads to  $b$ -dependent neutron transition intensities.

The  $T_h$ -symmetry CEF excitation spectrum has not been considered in detail in the literature, and the corresponding neutron transition intensities between  $T_h$  CEF levels have not been considered at all. To aid in the interpretation of our neutron scattering data we carried out these CEF calculations using a point charge model. We assumed an expansion of the perturbing CEF potential in spherical harmonics,

$$V(\Omega) = \sum_{\ell=4,6} g_\ell \sum_{m=-\ell}^{\ell} M_{\ell m} Y_{\ell m}(\Omega), \quad (1)$$

where the interaction strengths  $g_4$  and  $g_6$  are treated as free parameters. The spherical harmonic moments  $\{M_{\ell m}\}$  are determined by the positions of the 12 As ions, which we assigned the (scaled) coordinates  $\vec{x} = (\pm 1, \pm b, 0)$ ,  $(0, \pm 1, \pm b)$ ,  $(\pm b, 0, \pm 1)$ . The nonzero independent moments for  $\ell = 4, 6$  are  $M_{40} = 21(1 - 3b^2 + b^4)/2\sqrt{\pi}(1 + b^2)^2$ ,  $M_{60} = 3\sqrt{13}(2 - 17b^2 + 2b^4)/8\sqrt{\pi}(1 + b^2)^2$  and  $M_{66} = -15\sqrt{3003}b^2(1 - b^2)/16\sqrt{\pi}(1 + b^2)^3$ . The nonzero  $M_{66}$  for  $b \neq 1$  ( $T_h$  symmetry) confirms the presence of the  $B_6^6$  terms of Takegahara *et al.* [Eq.(7) of Ref.<sup>25</sup>], in addition to the usual  $B_4^4$  and  $B_6^6$   $O_h$ -symmetry terms. (Note that the  $T_h$ -allowed moment  $M_{66}$  vanishes at the  $O_h$ -symmetry point  $b = 1$ .) We also confirmed that the other nonzero moments satisfy the ratios quoted in Eq.(7) of Ref.<sup>25</sup>. Unlike Takegahara *et al.*<sup>25</sup>, we do not introduce a new parameter  $y$  for the  $T_h$ -symmetry terms, because they are completely determined by  $g_6$  and the lattice parameter  $b$  in the point charge model. This was previously noted by Goremychkin *et al.*<sup>18</sup>.

Diagonalization of this  $T_h$  CEF interaction within the  $\text{Pr}^{3+} {}^3\text{H}_4$  nonet gives our results for the spectrum of CEF levels and their associated eigenvectors. These eigenvectors depend only on the ratio  $g_6/g_4$  and the lattice parameter  $b$ ; the energies in addition have an arbitrary overall scale. Our results for the spectrum for  $b = 1$  ( $O_h$  symmetry) and  $b = 0.4267$  ( $\text{PrOs}_4\text{As}_{12}$  geometry) are shown in Figs. 1(b) and 1(d), using LLW normalization conventions<sup>26</sup>. (These conventions set our two Hamiltonian parameters in Eq.(1) to  $g_4 = (968\pi/21)x$  and  $g_6 = (-5808\pi/221)(1 - |x|)$ .) Note that the  $b = 1$

and  $b = 0.4267$  level schemes differ qualitatively, which demonstrates the importance of the  $T_h$  terms in this problem.

We find that the  $O_h$  singlet and doublet energy eigenvectors are unmodified by the  $T_h$  interaction, consistent with Takegahara *et al.*<sup>25</sup>. The singlet eigenvector (in a  $J_z^{\text{tot}}$  basis) is  $|\Psi_1\rangle = \sqrt{7/12}|0\rangle + \sqrt{5/24}(|4\rangle + |-4\rangle)$  and the two doublet states are  $|\Psi_{23a}\rangle = -\sqrt{5/12}|0\rangle + \sqrt{7/24}(|4\rangle + |-4\rangle)$  and  $|\Psi_{23b}\rangle = \sqrt{1/2}(|2\rangle + |-2\rangle)$ , consistent with earlier (numerical) results<sup>25,26</sup>. The singlet and doublet energy eigenvalues in our conventions are modified by the  $T_h$  interaction. In terms of the LLW variable  $x$ <sup>26</sup> and our parameter  $b$  they are  $E_1 = -(16/13(1 + b^2)^2)(91x(1 - 3b^2 + b^4) - 20(1 - |x|)(2 - 17b^2 + 2b^4))$  and  $E_{23} = -(16/13(1 + b^2)^2)(13x(1 - 3b^2 + b^4) + 16(1 - |x|)(2 - 17b^2 + 2b^4))$ . The corresponding analytic results for the two  $T_h$  triplet states for general  $b$  are quite complicated, so we only present numerical results for these states.

The neutron transition intensities are defined by  $I_{if} = |\langle f | J_z^{\text{tot}} | i \rangle|^2$ , as introduced by Birgeneau<sup>27</sup>. (There is an implicit sum over initial and final magnetic quantum numbers.) Our  $T_h$ -symmetry results for these quantities are shown in Fig. 5(a). The values in the limits  $x = \pm 1$  (no  $\ell = 6$  term, hence  $O_h$  symmetry) implicitly check Birgeneau's numerical  $O_h$  results; see the off-diagonal entries in his Table 1(e). These  $O_h$  limits are indicated on the vertical axis of Fig. 5(a).

Next we compare the observed CEF levels and their neutron excitation intensities to the well-known LLW CEF results for  $O_h$  symmetry [Fig. 1(b)] and our calculated CEF predictions for  $\text{PrOs}_4\text{As}_{12}$  under  $T_h$  symmetry [Fig. 1(d) and Fig. 5(a)]. Both  $O_h$  and  $T_h$  CEF spectra have  $x$  values that can accommodate a magnetic triplet ground state and a nearly degenerate singlet first excited state [vertical lines in Figs. 1(b) and 1(d)]. However, it is evident that the  $O_h$  scheme cannot explain the data because the observed 0.4 meV transition  $\Gamma_4^{(2)} \rightarrow \Gamma_1$  is incorrectly predicted to have zero intensity due to the  $O_h$  symmetry. While in the  $T_h$  scheme the relative neutron excitation strengths of the higher levels (at 13 and 23 meV) predicted in Fig. 1(d) seem to be in good agreement with observation at low temperatures, the As CEF alone predicts an incorrect spectrum of levels [Fig. 1(d)], with the triplet  $\Gamma_4^{(1)}$  being the highest excitation. The calculated neutron transition intensity shown in Fig. 5(a) can not explain the observed intensity at higher temperatures. As temperature increases, the excited states get populated and the excitations start to decrease in intensities. Meanwhile the new excited-state transitions start to increase. If  $\Gamma_4^{(1)}$ , instead of  $\Gamma_{23}$ , is the highest level, the intensity at 12.6 meV would not increase but that at 22.6 meV would, because the  $\Gamma_1$  to  $\Gamma_{23}$  transition is not allowed even in  $T_h$  symmetry. Goremychkin *et al.*<sup>18</sup> showed that the highest level in the similar Sb material is the  $\Gamma_{23}$  doublet.

## B. Combined Os – As CEF model

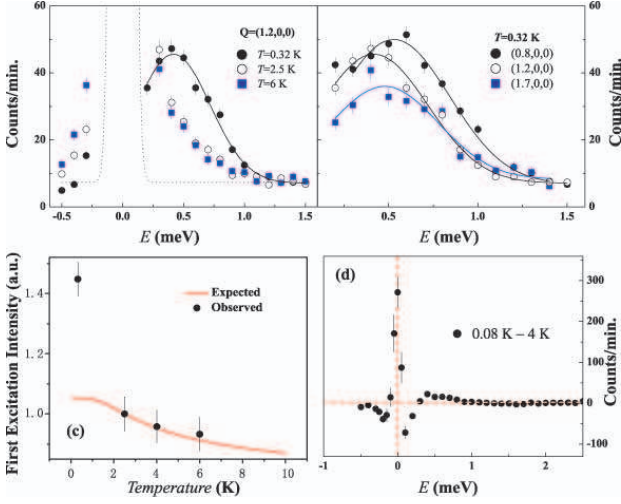


FIG. 3: (Color online) (a) Low energy spectrum of CEF excitations observed at  $T = 0.32, 2.5$  and  $6.0$  K using the SPINS spectrometer at NCNR. (b) The wave vector dependence of the excitations at  $Q = (0.8, 0, 0)$ ,  $Q = (1.2, 0, 0)$ , and  $Q = (1.7, 0, 0)$ . (c) The expected and observed temperature dependence of the intensity of the  $0.4$  meV mode. (d) The temperature difference spectrum between  $0.08$  K and  $4$  K, showing clear reduction in magnetic elastic scattering.

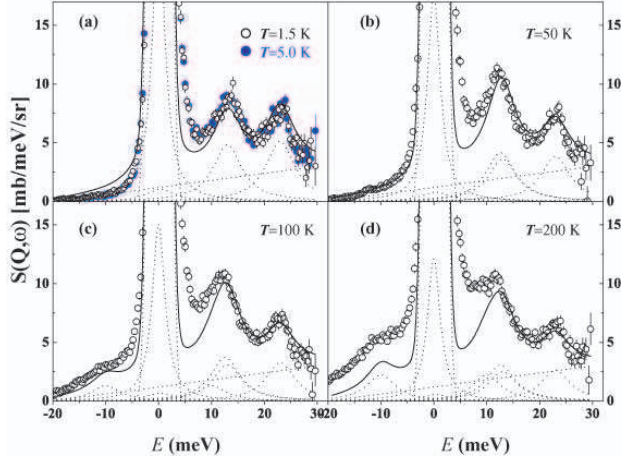


FIG. 4: (Color online) The temperature dependence of the excitations observed on HET with  $E_i = 32$  meV at (a)  $T = 1.5$  K,  $5$  K; (b)  $50$  K; (c)  $100$  K, and (d)  $200$  K. The lines are theoretical results for neutron excitation intensities, from the combined Os-As CEF model, with an arbitrary overall scale factor.

The twin constraints of having the  $\Gamma_{23}$  level at the top of the spectrum *and* having a large  $\Gamma_4^{(2)} \leftrightarrow \Gamma_1$  neutron excitation strength requires both Os and As terms in the CEF interaction. We therefore introduce a combined Os-As Hamiltonian,

$$H = H(\text{Os}) + H(\text{As}). \quad (2)$$

Although this model nominally has four parameters ( $g_4^{\text{Os}}, g_6^{\text{Os}}, g_4^{\text{As}}$  and  $g_6^{\text{As}}$ ), only three are independent;

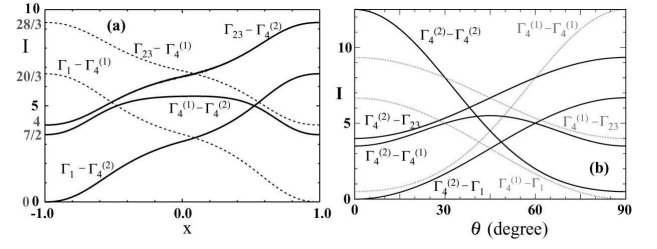


FIG. 5: (a) The theoretical neutron transition intensity for As CEF alone with  $b=0.4267$ . (b) Neutron excitation intensities predicted by the combined Os-As CEF model.

$g_4^{\text{Os}}$  and  $g_4^{\text{As}}$  cannot be distinguished because they are summed into a single coefficient of the  $O_h$ -symmetry  $\ell = 4$  interaction. For this reason we introduce combined  $O_h$ -symmetry Os-As coefficients  $g_4 = g_4^{\text{Os}} + g_4^{\text{As}}$  and  $g_6 = g_6^{\text{Os}} + g_6^{\text{As}}$ , which we normalize according to LLW conventions. As the  $\ell = 6$   $T_h$ -symmetry terms from  $H(\text{As})$  in the CEF are proportional to  $g_6^{\text{As}}$  alone, the strengths  $g_6^{\text{Os}}$  and  $g_6^{\text{As}}$  can be distinguished. We parametrize these two  $\ell = 6$  interactions using the total  $O_h$ -symmetry  $g_6$  and a  $T_h/O_h$  relative strength  $r_6$ , which is the ratio of the coefficients of  $Y_{62}$  to  $Y_{60}$  in the CEF potential. The energy levels of this Hamiltonian are  $E_{4(2)} = -6g_4 - 8g_6 - f$ ,  $E_1 = 28g_4 - 80g_6$ ,  $E_{4(1)} = -6g_4 - 8g_6 + f$  and  $E_{23} = 4g_4 + 64g_6$ , where  $f = ((20g_4 + 12g_6)^2 + 960r_6^2g_6^2)^{1/2}$ . For  $r_6 = 0$  these reduce to the familiar LLW  $O_h$  spectrum. In the pure As model,  $r_6$  is determined by CEF theory if we assume point As ions, and is given by  $(11\sqrt{105}/4)b^2(1-b^2)/(1+b^2)(1-(17/2)b^2+b^4)$ . For  $\text{PrOs}_4\text{As}_{12}$  we have  $b = 0.4267$ , which gives a rather large  $r_6 = -6.901$ . This drives strong level repulsion between the two triplets, which explains why the pure As spectrum of Fig.1d differs so greatly from the  $O_h$  (pure Os) symmetry spectrum of Fig.1b.

Our experimentally observed CEF levels are close to but not exactly consistent with the predictions above of the mixed Os-As model, since the gap ratio  $(E_{4(1)} - E_{4(2)})/(E_{23} - E_{4(2)}) \approx 0.57$  is slightly *below* the theoretical lower bound of  $7/12$ . The parameters we estimate from the measured gaps are  $g_4 \approx 0.24$  meV and  $g_6 \approx 0.20$  meV. The value of  $r_6$  is not determined by the measured energies due to the inconsistency mentioned above, although  $r_6 \lesssim 0.5$  appears plausible. A more sensitive determination of  $r_6$  is possible through the measurement of the inelastic neutron excitation intensities we discuss below.

The neutron excitation intensities in this combined Os-As Hamiltonian depend only on a single parameter  $\theta$ , which is the mixing angle of the triplet energy eigenvectors when expanded in an  $O_h$ -symmetry  $|3\rangle, |3'\rangle$  basis,

$$\begin{aligned} |4(1)\rangle &= +\sin(\theta)|3\rangle + \cos(\theta)|3'\rangle \\ |4(2)\rangle &= +\cos(\theta)|3\rangle - \sin(\theta)|3'\rangle. \end{aligned} \quad (3)$$

This mixing angle is related to the Hamiltonian param-



eters by  $\tan(2\theta) = 2\sqrt{15}r_6/(5(g_4/g_6) + 3)$ . The singlet and doublet  $O_h$  energy eigenvectors are unchanged. The nonzero neutron excitation intensities in terms of  $s = \sin(\theta)$  and  $c = \cos(\theta)$  are  $\Gamma_4^{(2)} \leftrightarrow \Gamma_1 = (20/3)s^2$ ,  $\Gamma_4^{(2)} \leftrightarrow \Gamma_4^{(1)} = 7/2 + 8c^2s^2$ ,  $\Gamma_4^{(2)} \leftrightarrow \Gamma_{23} = 4 + (16/3)s^2$ ,  $\Gamma_1 \leftrightarrow \Gamma_4^{(1)} = (20/3)c^2$ ,  $\Gamma_4^{(1)} \leftrightarrow \Gamma_{23} = 28/3 - (16/3)s^2$ ,  $\Gamma_4^{(2)} \leftrightarrow \Gamma_4^{(2)} = (25/2)(1 - (4/5)s^2)^2$ , and  $\Gamma_4^{(1)} \leftrightarrow \Gamma_4^{(1)} = (1/2)(1 + 4s^2)^2$ . The calculated neutron scattering intensity of different transitions as a function of  $\theta$  is shown in Fig. 5(b). We recover the  $O_h$ -symmetry results of Birgeneau (Table 1(e) of Ref.<sup>27</sup>) for  $s = 0, c = 1$ .

We carried out a least-squares fit of our neutron excitation data at 1.5 K, 50 K, 100 K and 200 K (Fig. 4) to the theoretical intensities given above, which gives an estimate of the triplet mixing angle  $\theta$  in  $\text{PrOs}_4\text{As}_{12}$ ,

$$\theta \approx 22.5^\circ. \quad (4)$$

When combined with the values of  $g_4$  and  $g_6$  from the spectrum, this  $\theta$  corresponds to  $r_6 \approx 1.2$ . In this fit the relatively isolated  $\Gamma_4^{(2)} \rightarrow \Gamma_4^{(1)}$  peak at 23 meV was used to infer the background, which was taken to be constant plus linear. The assumed lineshapes were Lorentzians with a common linewidth, fixed by the 23 meV peak. The calculated intensities of the individual transitions (dotted lines) and the total intensity (solid lines) for each temperature are shown in Figs. 4(a)-(d). We note that the intensity reduction at 0.4 meV on warming from 0.32 K to 2.5 K is larger than that expected from the CEF model [Fig. 3(c)], thus suggesting Pr-Pr interactions below  $T_N$  ( $=2.3$  K) are important. On the other hand, the large difference between the calculated and expected intensity around 8 meV in the 200 K data is presumably due to thermally populated phonons (Fig. 2a).

### C. Field effect on the CEF gap

If the ground state of  $\text{PrOs}_4\text{As}_{12}$  is indeed the  $\Gamma_4^{(2)}$  triplet, application of a magnetic field should Zeeman split it, resulting in a field dependent energy gap. There should also be a reduction in the intensity of the zero-energy  $\Gamma_4^{(2)} \rightarrow \Gamma_4^{(2)}$  magnetic scattering. Figure 6 shows that these expectations are indeed qualitatively satisfied. The first excited state at 0.4 meV shifts toward higher energies as the applied field increases. The field-dependent transition energy is linear only at higher fields (between 6 T and 11 T). The drop of intensity in the elastic channel is almost constant for all applied fields, as shown in the inset of Fig. 6(b). Figure 6(c) shows that the wave vector dependence is also present with applied magnetic field ( $H = 9$  T). Normally the field-splitting of the ground state multiplet would be a very clear test of our  $\Gamma_4^{(2)}$  triplet assignment for the ground state. However,  $\text{PrOs}_4\text{As}_{12}$  is complicated by the near degeneracy of the  $\Gamma_4^{(2)}$  and  $\Gamma_1$  levels, which mix strongly under an applied field. This results in a more complicated spectrum of low-lying states, with several low-field level crossings and

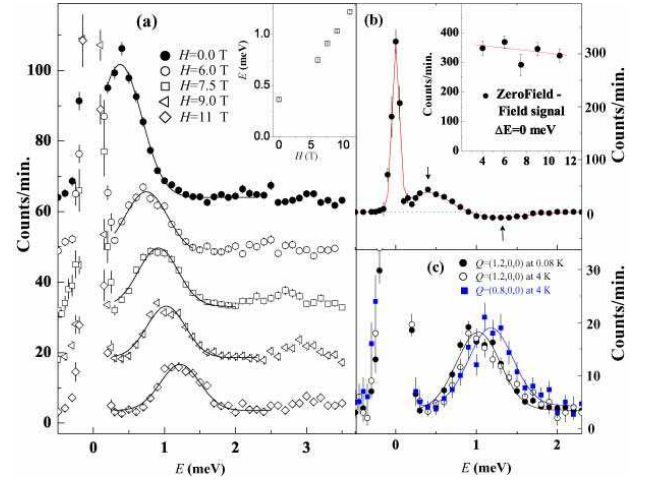


FIG. 6: (Color online) (a) The magnetic field dependence of the low-lying CEF excitations at  $Q = (1.2, 0, 0)$  and  $T = 0.08$  K. The inset shows the field dependence of the first excited state. (b) The difference spectrum between 0 T and 11 T at  $Q = (1.2, 0, 0)$  and  $T = 0.08$  K. The effect of an applied field is to suppress intensity at  $\hbar\omega = 0$  meV, and to split the spin-triplet ground state; the latter results in the field dependence of the 0.4 meV peak in (a), which may involve an intra-triplet transition. The elastic intensity suppression effect essentially disappears for fields above 4 T. (c) The field-induced CEF excitation at  $\approx 1.1$  meV is weakly wave vector dependent, and shows essentially no temperature dependence between  $T = 0.08$  K and 4 K.

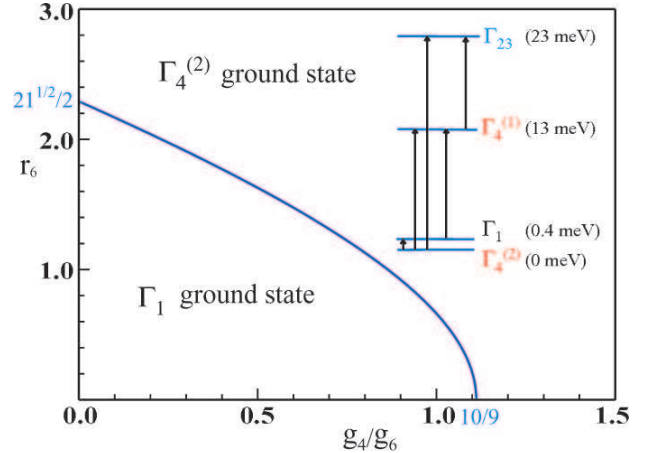


FIG. 7: (Color online) The boundary between singlet and triplet ground states in skutterudites ( $E_1 = E_4^{(2)}$ ) as a function of  $r_6$  and  $g_4/g_6$ , and the observed  $\text{PrOs}_4\text{As}_{12}$  spectrum.

neutron scattering intensities that are also modified by their field-induced  $\Gamma_4^{(2)}-\Gamma_1$  mixing.

Our determination of the CEF levels in  $\text{PrOs}_4\text{As}_{12}$  reveals the reasons for the wide range of behaviours in different FS. The spectrum of CEF levels is largely determined by the  $O_h$  symmetry field of the eight nearest neighbor ions, and for Os the near equality of the  $\ell = 4$  and  $\ell = 6$  strengths  $g_4$  and  $g_6$  implies nearly degener-

ate low-lying singlet (insulator) and triplet (AF) levels. The low temperature magnetic properties are determined by which of these phases happens to be the true ground state. In the CEF model, this is specified by the two parameters  $g_4/g_6$  and  $r_6$  (Fig. 7); in  $\text{PrOs}_4\text{As}_{12}$ , which has a triplet ground state, we estimate  $g_4/g_6 \approx 1.15$  and  $r_6 \approx 1.2$ . The  $T_h$  symmetry pnictogen CEF (proportional to  $r_6$ ) acts to stabilize the triplet state, and can itself lead to a triplet ground state if  $r_6$  is sufficiently large to cross the phase boundary shown in Fig. 7.

In principle, one can extend our approach to calculate the ground states of other Pr-FS by determining its crystal structure and  $g_4/g_6$  ratio. The necessity of using the  $T_h$ -symmetry of As rather than the  $O_h$ -symmetry pure Os form to explain the observed excitations shows that the detailed pnictogen geometry is important in determining the CEF levels. Indeed, the AF-ordered ground state in  $\text{PrOs}_4\text{As}_{12}$  can arise from a  $\Gamma_4^{(2)}$  triplet magnetic ground state, while the superconducting  $\text{PrOs}_4\text{Sb}_{12}$  has nonmagnetic  $\Gamma_1$  singlet ground state. The nearly degenerate first excited state  $\Gamma_1$  at 0.4 meV ( $\sim 4$  K), and its temperature and field dependence (Figs. 4 and 6), may explain the presence of multiple transitions in the specific heat (in  $C(T)/T$  versus  $T$ ) and its field dependence<sup>14,15,22</sup>.

## II. SUMMARY

To understand the observed  $\text{Pr}^{3+}$  CEF levels, one

must incorporate the As ions' contribution to the CEF Hamiltonian<sup>24,25</sup>, in addition to the usual Os cubic field terms. A comparison of our CEF calculations using this more general Hamiltonian with our experimental results shows that the  $\text{Pr}^{3+}$  CEF level scheme in  $\text{PrOs}_4\text{As}_{12}$  consists of a  $\Gamma_4^{(2)}$  magnetic triplet ground state, a nearly degenerate  $\Gamma_1$  singlet excitation, and higher  $\Gamma_4^{(1)}$  magnetic triplet and  $\Gamma_{23}$  nonmagnetic doublet excited states. We find that contributions in the CEF Hamiltonian due to As are important in determining the neutron excitation intensities in  $\text{PrOs}_4\text{As}_{12}$ ; our results differ qualitatively from the predictions of the conventional CEF Hamiltonian<sup>26,27</sup>, and therefore provide a microscopic understanding for its AF ground state.

## ACKNOWLEDGEMENT

We thank R. J. Birgeneau, B. C. Sales and D. Schultz for helpful discussion. The work at UT/ORNL was supported by the U.S. DOE under grant DE-FG02-05ER46202, ORNL is managed by UT-Battelle, LLC, for the U.S. DOE under contract DE-AC05-00OR22725. Work at UCSD was supported by the U.S. DOE under grant DE-FG02-04ER46105 and by the NSF under grant DMR-0335173. Work on SPINS was supported in part by the National Science Foundation under Agreement No. DMR-0454672.

- 
- <sup>1</sup> G. S. Nolas and G. Fowler, *Ann. Rev. Mater. Sci.* **29**, 89 (1999).
  - <sup>2</sup> B. C. Sales, in *Handbook on the Physics and Chemistry of Rare Earths*, Vol 33, Ch. 211, pp.1-34. (eds. K. A. Gschneidner, Jr., J.-C. G. Bünzli and V. K. Pecharsky) (Elsevier Science, 2003).
  - <sup>3</sup> B. C. Chakoumakos and B. C. Sales, *J. Alloys and Compounds* **407**, 87 (2006).
  - <sup>4</sup> Y. Aoki, T. Namiki, T. D. Matsuda, K. Abe, H. Sugawara, and H. Sato, *Phys. Rev. B* **65**, 064446 (2002).
  - <sup>5</sup> H. Sugawara, T. D. Matsuda, K. Abe, Y. Aoki, H. Sato, S. Nojiri, Y. Inada, R. Settai, and Y. Ōnuki, *Phys. Rev. B* **66**, 134411 (2002).
  - <sup>6</sup> C. Sekine, T. Uchiumi, I. Shirotni, and T. Yagi, *Phys. Rev. Lett.* **79**, 3218 (1997).
  - <sup>7</sup> M. Matsunami, L. Chen, H. Okamura, T. Nanba, C. Sekine and I. Shirotni, *J. Magn. Magn. Mater.* **272-276**, E39 (2004).
  - <sup>8</sup> M. Yogi, H. Kotegawa, Y. Imamura, G. -q. Zheng, Y. Kitaoka, H. Sugawara, and H. Sato, *Phys. Rev. B* **67** 180501 (2003).
  - <sup>9</sup> N. Takeda and M. Ishikawa, *J. Phys. Soc. Jpn.* **69** 868 (2000).
  - <sup>10</sup> E. D. Bauer, N. A. Frederick, P. -C. Ho, V. S. Zapf, and M. B. Maple, *Phys. Rev. B* **65** 100506(R) (2002).
  - <sup>11</sup> M. B. Maple, E. D. Bauer, V. S. Zapf, E. J. Freeman, N. A. Frederick and R. P. Dickey, *Acta Phys. Pol. B* **32**, 3291 (2001).
  - <sup>12</sup> E. D. Bauer, St. Berger, Ch. Paul, M. Della Mea, G. Hilscher, H. Michor, M. Reissner, W. Steiner, A. Grytsiv, P. Rogl, and E. W. Scheidt, *Phys. Rev. B* **66**, 214421 (2002).
  - <sup>13</sup> N. P. Butch, W. M. Yuhasz, P. -C. Ho, J. R. Jeffries, N. A. Frederick, T. A. Sayles, X. G. Zheng, M. B. Maple, J. B. Betts, A. H. Lacerda, F. M. Woodward, J. W. Lynn, P. Rogl, and G. Giester, *Phys. Rev. B* **71**, 214417 (2005).
  - <sup>14</sup> W. M. Yuhasz, N. P. Butch, T. A. Sayles, P. -C. Ho, J. R. Jeffries, T. Yanagisawa, N. A. Frederick, M. B. Maple, Z. Henkie, A. Pietraszko, S. K. McCall, M. W. McElfresh, and M. J. Fluss, *Phys. Rev. B* **73**, 144409 (2006).
  - <sup>15</sup> M. B. Maple, N. P. Butch, N. A. Frederick, P. -C. Ho, J. R. Jeffries, T. A. Sayles, T. Yanagisawa, W. M. Yuhasz, Songxue Chi, H. J. Kang, J. W. Lynn, Pengcheng Dai, S. K. McCall, M. W. McElfresh, M. J. Fluss, Z. Henkie, and A. Pietraszko, *PNAS* **103**, 6783 (2006).
  - <sup>16</sup> D. T. Adroja, J. -G. Park, E. A. Goremychkin, N. Takeda, M. Ishikawa, K. A. McEwen, R. Osborn, A. D. Hillier, and B. D. Rainford, *Physica B* **359-361**, 983 (2005).
  - <sup>17</sup> D. L. Cox and A. Zawakowski, *Adv. Phys.* **47**, 599 (1998).
  - <sup>18</sup> E. A. Goremychkin, R. Osborn, E. D. Bauer, M. B. Maple, N. A. Frederick, W. M. Yuhasz, F. M. Woodward, and J. W. Lynn, *Phys. Rev. Lett.* **93**, 157003 (2004).
  - <sup>19</sup> K. Kuwahara, K. Iwasa, M. Kohgi, K. Kaneko, S. Araki, N. Metoki, H. Sugawara, Y. Aoki and H. Sato, *J. Phys. Soc. Jpn.* **73**, 1438 (2004).
  - <sup>20</sup> K. Kuwahara, K. Iwasa, M. Kohgi, K. Kaneko, N. Metoki,

- S. Raymond, M. -A. Méasson, J. Flouquet, H. Sugawara, Y. Aoki, and H. Sato, Phys. Rev. Lett. **95**, 107003 (2005).
- <sup>21</sup> Y. Aoki, T. Namiki, S. Ohsaki, S. R. Saha, H. Sugawara, and H. Sato, J. Phys. Soc. Jpn. **71**, 2098 (2002).
- <sup>22</sup> Pei-chun Ho, J. Singleton, M. B. Maple, H. Harima, P. A. Goddard, Z. Henkie, and A. Pietraszko, New J. Phys. **9**, 269 (2007).
- <sup>23</sup> S. D. Wilson, Pengcheng Dai, D. T. Adroja, S. -H. Chung, J. W. Lynn, N. P. Butch, and M. B. Maple, Phys. Rev. Lett. **94**, 056402 (2005).
- <sup>24</sup> K. Takegahara, J. Phys. Soc. Jpn. **69**, 1572 (2000).
- <sup>25</sup> K. Takegahara, H. Harima, and A. Yanase, J. Phys. Soc. Jpn. **70**, 1190 (2001).
- <sup>26</sup> K. R. Lea, M. J. M. Leask, and W. P. Wolf, J. Phys. Chem. Solids **23**, 1381 (1962).
- <sup>27</sup> R. J. Birgeneau, J. Phys. Chem. Solids **33**, 59 (1972).